BIOCHEMISTRY
including biophysical chemistry & molecular biology
Article

Biochemistry **2011,** *50,* 367–375 367
DOI: 10.1021/bi1016843

Kinetic and Chemical Mechanism of the Dihydrofolate Reductase from *Mycobacterium tuberculosis*[†]

Clarissa M. Czekster, An Vandemeulebroucke, and John S. Blanchard*

Department of Biochemistry, Albert Einstein College of Medicine, 1300 Morris Park Avenue, Bronx, New York 10461, United States

Received October 19, 2010; Revised Manuscript Received November 30, 2010

ABSTRACT: Dihydrofolate reductase from *Mycobacterium tuberculosis* (*Mt*DHFR) catalyzes the NAD(P)-dependent reduction of dihydrofolate, yielding $NAD(P)^+$ and tetrahydrofolate, the primary one-carbon unit carrier in biology. Tetrahydrofolate needs to be recycled so that reactions involved in dTMP synthesis and purine metabolism are maintained. In this work, we report the kinetic characterization of the *Mt*DHFR. This enzyme has a sequential steady-state random kinetic mechanism, probably with a preferred pathway with NADPH binding first. A pK_a value for an enzymic acid of approximately 7.0 was identified from the pH dependence of V, and the analysis of the primary kinetic isotope effects revealed that the hydride transfer step is at least partly rate-limiting throughout the pH range analyzed. Additionally, solvent and multiple kinetic isotope effects were determined and analyzed, and equilibrium isotope effects were measured on the equilibrium constant. ^{D_2O}V and $^{D_2O}V/K_{[4R\text{-}4\text{-}^2H]NADH}$ were slightly inverse at pH 6.0, and inverse values for $^{D_2O}V_{[4R\text{-}4\text{-}^2H]NADH}$ and $^{D_2O}V/K_{[4R\text{-}4\text{-}^2H]NADH}$ suggested that a pre-equilibrium protonation is occurring before the hydride transfer step, indicating a stepwise mechanism for proton and hydride transfer. The same value was obtained for ^Dk_H at pH 5.5 and 7.5, reaffirming the rate-limiting nature of the hydride transfer step. A chemical mechanism is proposed on the basis of the results obtained here.

Tuberculosis (TB)[1] is a global health concern. It is estimated that one-third of humanity is infected with TB and that 1.7 million deaths occur each year (*1*). Despite global efforts to contain the disease, the number of TB cases is still increasing, and the appearance of strains resistant to first-line drugs (MDR-TB) and to both first- and second-line drugs (XDR-TB) has intensified the search for new and more effective antibacterial agents (*2*).

Dihydrofolate reductase (DHFR) catalyzes the NADPH-dependent reduction of dihydrofolate (DHF), yielding tetrahydrofolate (THF), an important reaction in the folate cycle, which supplies one-carbon units for the biosynthesis of deoxythymidine monophosphate (dTMP), and for reactions involved in the biosynthesis of purines (Scheme 1). Inhibition of the folate cycle interrupts the supply of dTMP and halts DNA synthesis and, consequently, cell proliferation. Drugs that inhibit DHFR have been used for decades to treat cancer (methotrexate and pemetrexate), bacterial infections (trimethoprim), and malaria (pyrimethamine) (*3*). Recently, a series of structure-based inhibitors were designed for the DHFR from *Mycobacterium tuberculosis* (*Mt*DHFR) (*4*−*6*), but a preliminary assessment of the chemotherapeutic potential of those compounds reveals that they lack the solubility, potency, and specificity required for a new drug targeting this enzyme.

The chemical mechanism of the DHFR-catalyzed reaction continues to be debated, especially the order of the protonation and hydride transfer steps, the identity of the group whose pK_a value is observed in the V−pH profiles, and the involvement of a water molecule in the protonation step, even though DHFRs from numerous prokaryotic and eukaryotic organisms have been studied for the past 50 years. The majority of the experimental and theoretical data favors the protonation step preceding the hydride transfer step in the *Ec*DHFR-catalyzed reaction, and the idea that a network of water molecules linked to a general acid would be promoting the protonation (*7*−*9*). Alternatively, some authors argue that protonation at O4 would facilitate transfer of the hydride to C6 and the subsequent N5 ring nitrogen protonation (*8*, *10*, *11*). Recently, work conducted with DHFR from *Thermotoga maritima* (*Tm*DHFR) suggested that the two steps (N5 protonation and C6 hydride transfer) were occurring in a concerted manner (*12*), suggesting diversity in terms of chemical mechanism for the same enzyme-catalyzed reaction.

In this work, the kinetic and chemical mechanisms of *Mt*DHFR were investigated using initial velocity and pH−rate profiles studies, measuring kinetic isotope effects under steady-state and pre-steady-state conditions, as well as equilibrium isotope effects. A chemical mechanism is proposed on the basis of the results obtained.

EXPERIMENTAL PROCEDURES

Materials. All chemicals were of analytical or reagent grade and were used without further purification. Deuterium oxide (99.9 at. % D) was from Cambridge Isotope Laboratories.

[†]This work was supported by National Institutes of Health Grant AI33696.

*To whom correspondence should be addressed: Department of Biochemistry, Albert Einstein College of Medicine, 1300 Morris Park Ave., Bronx, NY 10461. Phone: (718) 430-3096. Fax: (718) 430-8565. E-mail: blanchar@aecom.yu.edu.

[1]Abbreviations: TB, tuberculosis; MDR-TB, multidrug resistant tuberculosis; XDR-TB, extensively drug resistant tuberculosis; *Mt*DHFR, dihydrofolate reductase from *Mycobacterium tuberculosis* H37Rv; DHF, dihydrofolate; THF, tetrahydrofolate; NADPH, nicotinamide adenine dinucleotide phosphate (reduced form); NADH, nicotinamide adenine dinucleotide (reduced form); NADL, NADH or [4*R*-4-^{2}H]NADH used as a substrate; dTMP, deoxythymidine monophosphate; KIE, kinetic isotope effect; SKIE, solvent kinetic isotope effect; MKIE, multiple kinetic isotope effect; EIE, equilibrium isotope effect; *Ec*DHFR, DHFR from *Escherichia coli*; *Sp*DHFR, DHFR from *Streptococcus pneumoniae*; *Tm*DHFR, DHFR from *Thermatoga maritima*.

Published on Web 12/07/2010

Scheme 1: Reaction Catalyzed by DHFR

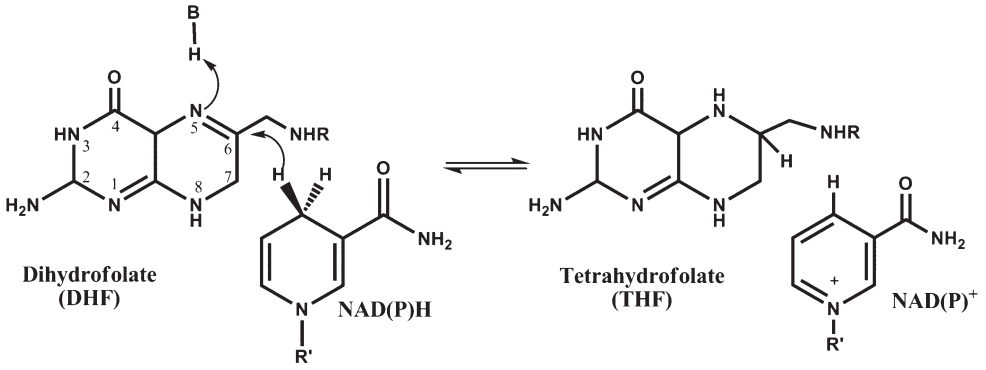

Reaction catalyzed by DHFR.

Purification of MtDHFR. Competent *Escherichia coli* BL21(DE3) cells (Novagen) were transformed with recombinant plasmid pET28a(+):*dfrA*, and the expression and purification of *Mt*DHFR followed the protocol previously reported (*13*). Protein concentrations were determined by using the theoretical ε_{280} value of 40450 M^{-1} cm^{-1} or an ε_{340} of 6220 M^{-1} cm^{-1} due to bound NADPH (*14*).

Preparation of the MtDHFR−NADP$^+$ Complex. Because DHFR is present in a complex with NADPH after its purification and this tightly bound NADPH could not be removed by extensive dialysis, a form of the enzyme that had $NADP^+$ instead of NADPH was generated. The *Mt*DHFR−NADPH complex was immobilized onto a Ni-NTA resin, and 10 mL of 100 mM $NADP^+$ was passed through the column, to form the *Mt*DHFR−$NADP^+$ form of the enzyme. The enzyme was eluted with 500 mM imidazole, dialyzed against 2 × 2 L of 100 mM HEPES (pH 7.5), and frozen at −80 °C. Attempts to generate the apoenzyme were unsuccessful, because the enzyme obtained after denaturation and refolding was less active and prone to precipitation.

Preparation of [4R-4-^{2}H]NAD(P)H. [4*R*-4-^{2}H]NADH was prepared using formate dehydrogenase and deuterated formic acid (*15*); [4*R*-4-^{2}H]NADPH was prepared using alcohol dehydrogenase from *Thermoanaerobium brockii*, and 2-propanol-d_8 (*16*). All pyridine nucleotides, including commercially available NADH and NADPH to be used in isotope effect experiments, were purified with a Mono-Q column equilibrated with water, using a linear gradient of 1 M sodium bicarbonate for elution (at 0.66%/mL). Fractions with an 260 nm:340 nm absorption ratio of ≤2.3 were pooled, fast frozen, and lyophilized.

Enzymatic Assay for MtDHFR. Assays were performed under initial rate conditions at 25 °C and 100 mM HEPES (pH 7.5), unless stated otherwise. Measurements were performed in at least duplicate. The reaction was started by the addition of 10 nmol of *Mt*DHFR, and the decrease in absorbance due to NAD(P)H oxidation and DHF reduction was measured at 340 nm, at 25 °C for 1 min. A combined molar extinction coefficient value of 11800 M^{-1} cm^{-1} was used (*17*).

Initial Velocity and Product Inhibition Patterns. We determined apparent kinetic constants by fixing the concentration of one substrate at saturating levels and varying the concentration of the other substrate. An $_{app}K_{NADPH}$ of < 1 μM was estimated, too low to allow NADPH to be varied in initial velocity studies, and NADH was used instead. Initial velocity studies were conducted using five fixed concentrations of DHF while NADH concentrations were varied. Product inhibition experiments were conducted at varying concentrations of one substrate, fixed subsaturating concentrations of the other substrate, and different fixed concentrations of THF or $NADP^+$.

pH−Rate Profiles. To investigate the role of acid−base catalysis in the *Mt*DHFR-catalyzed reaction, the pH dependence of the kinetic parameters was determined by measuring initial rates at varying concentrations of one substrate and saturating concentrations of the other. The experiments were conducted throughout the pH range of 5.5−8.5, employing a mixed buffer system containing citric acid, HEPES, and TAPS. The pH stability of the enzyme was tested by incubating the enzyme in the desired buffer and conducting the standard assay using HEPES (pH 7.5).

Kinetic Isotope Effects. Primary kinetic isotope effects (KIEs) were measured using [4*R*-4-^{2}H]NADH or [4*R*-4-^{2}H]NADPH and DHF as substrates, with the same mixed buffer system used for the pH−rate profiles. A study of the dependence of $^DV/K$ on the concentration of the cosubstrate was conducted by using five fixed concentrations of DHF while varying the concentration of NADH or [4*R*-4-^{2}H]-NADH. Solvent kinetic isotope effects (SKIEs) were measured in either H_2O or 91 at. % D_2O, and initial velocities in the presence of a fixed concentration of one substrate and varying concentrations of the cosubstrate were obtained. Viscosity effects were evaluated by comparing the rates obtained in H_2O or 9% glycerol, which mimics the viscosity increase caused by D_2O (η_r = 1.24) (*18*). Multiple KIEs (MKIEs) were determined by measuring the SKIE using [4*R*-4-^{2}H]NADH as the substrate. To rule out the possibility that any change in velocity was being caused by pH fluctuations in the SKIE and MKIE measurements, we used citrate buffer (pL 6.0) because this value is located in a plateau region identified in the pH−rate profile studies.

Equilibrium Isotope Effects (EIE). Equilibrium isotope effects were determined in water or D_2O ($^{D_2O}K_{eq}$), and using NADH or [4*R*-4-^{2}H]-NADH as the substrate ($^DK_{eq}$) (*19*). Each reaction mixture contained 100 μM DHF and 100 μM NADH or [4*R*-4-^{2}H]NADH in citrate buffer (pH 6.0). The initial absorbance was recorded, and after that, 20 nM *Mt*DHFR was added (changing the reaction volume by no more than 1%) and the reaction was followed until the equilibrium was reached, usually for less than 1 h. The concentration of products and substrates in equilibrium was calculated by using the combined ε of 11800 M^{-1} cm^{-1} and using the initial and final absorbancies. Each value is the average of at least three measurements. All solvents and buffers were purged with argon before each measurement to delay THF oxidation (*20*).

Stopped-Flow Measurements. To better evaluate the rate-limiting nature of the chemical step, KIEs were measured under single-turnover conditions using the *Mt*DHFR−$NADP^+$ form of the enzyme. All measurements were conducted on a SX-20 stopped-flow spectrophotometer (Applied Photophysics) under pseudo-first-order conditions with an at least 5-fold excess of *Mt*DHFR over the limiting substrate (DHF). Assays contained 1 μM DHF, 100 μM NADPH or [4*R*-4-^{2}H]NADPH, and varied concentrations of *Mt*DHFR, to ensure that binding is not contributing to the observed rates. Measurements were performed at pH 5.5 and 7.5 using the same mixed buffer system employed in previous experiments.

Data Analysis. All data were fitted to the appropriate equations using the nonlinear regression function of SigmaPlot 2000 (SPSS, Inc.) or Origin 7.0 (OriginLab, Inc.).

Initial velocity kinetic data with one substrate fixed at a saturating concentration and varied concentrations of the other substrate were fitted to eq 1.

$$v = VA/(K + A) \quad (1)$$

Data for an intersecting initial velocity pattern were fitted to eq 2, which describes a sequential mechanism.

$$v = VAB/(K_{ia}K_b + K_aB + K_bA + AB) \quad (2)$$

Inhibition results were fitted to eq 3, describing competitive inhibition, or eq 4, for noncompetitive inhibition.

$$v = VA/[K(1 + I/K_{is}) + A] \quad (3)$$

$$v = VA/[K(1 + I/K_{is}) + A(1 + I/K_{ii})] \quad (4)$$

For eqs 1−4, V is the maximum velocity, A and B represent substrate concentrations, K_a and K_b are the Michaelis constants for substrates A and B, respectively, and K_{is} and K_{ii} are the slope and intercept inhibition constants, respectively.

pH−rate profiles were fitted to eq 5

$$\log y = \log[C/(1 + K_b/H)] \quad (5)$$

where y is the kinetic parameter, C is the pH-independent value of y, H is the proton concentration, and K_b is the apparent basic dissociation constant for ionizing groups.

The pH dependence of the kinetic isotope effect data was fitted to eq 6

$$Y = \frac{Y_L + Y_H(10^{-pK_a}/10^{-pH})}{1 + 10^{-pK_a}/10^{-pH}} \quad (6)$$

where Y_L and Y_H are the limiting values at low and high pH, respectively, and K_a is the dissociation constant for ionizable groups (*21*)

The kinetic isotope effect data were fitted to eq 7, which describes the effects on V/K on v. The $^D(V/K_{app})$ measured with five fixed concentrations of NADH or [4*R*-4-^{2}H]NADH and varying concentrations of DHF (50 points in total) were simultaneously fitted to eq 8, which assumes isotope effects on V, V/K_a, V/K_b, and K_{ia}. For eqs 7 and 8, F_i represents the fraction of isotopic label and $E_{V/K}$ and E_V are the isotope effects minus one on V/K and V, respectively.

$$v = VA/[K(1 + F_iE_{V/K}) + A(1 + F_iE_V) \quad (7)$$

$$v = VAB/\{[K_{ia}K_B(1 + F_iE_{K_{ia}}) + K_BA](1 + F_iE_{V/K_B}) + K_AB(1 + F_iE_{V/K_A}) + AB(1 + F_iE_V)\} \quad (8)$$

The notation utilized to express isotope effects is that of Northrop (*22*).

Single-turnover experiments were fitted to a single-exponential curve, represented by eq 9

$$y = y_0 + A_1e^{-kt} \quad (9)$$

where y_0 is the y offset, A_1 is the amplitude, and k is the observed rate constant.

The k_{obs} values obtained with different concentrations of enzyme were replotted as a function of enzyme concentration and fitted to eq 10 (*23*)

$$k_{obs} = k_HE/K_d + E \quad (10)$$

where k_{obs} is the observed rate constant after the single-exponential fitting at different concentrations of enzyme, k_H is the rate obtained with NADPH used as the substrate, E is the enzyme concentration, and K_d is the dissociation constant for the enzyme and the limiting substrate.

The isotope effect on the hydride transfer step (^Dk_H) was obtained by dividing k_H/k_D, using the values obtained after fitting with eq 10.

RESULTS AND DISCUSSION

Initial Velocity and Product Inhibition Patterns. The analysis of the initial velocity pattern obtained using NADH and DHF as substrates reveals that the *Mt*DHFR-catalyzed reaction has a sequential kinetic mechanism, with the formation of a ternary complex, as observed for DHFRs from other organisms (Figure 1). Because all lines intercept at the left of the y axis, a rapid-equilibrium ordered mechanism was ruled out. A k_{cat} of 1.6 ± 0.1 s^{-1} was determined, being very similar to the $_{app}k_{cat}$ of 2.3 ± 0.1 s^{-1} obtained when NADPH and DHF were used as substrates. Those values are 1 order of magnitude lower than those for the *E. coli* (*Ec*DHFR) and human (*Hs*DHFR) enzymes (*17*, *24*), and almost 20 times lower than those of the *Streptococcus pneumoniae* and mouse DHFRs (*25*, *26*). The K_m values for both NADPH and DHF are very low: $K_{DHF} = 1.6 \pm 0.4\,\mu$M, and $K_{NADPH} < 1\,\mu$M. It is common for DHFRs from other organisms to have at least one substrate with a K_m value in the low micromolar or submicromolar range. A higher value was obtained for K_{NADH} (69 ± 7 μM), demonstrating the important contribution of electrostatic interactions between the 2′-phosphate group and cationic side chains in the nucleotide binding pocket of the enzyme that differentiate between the two cofactors (*27*). Folate was tested as a substrate at concentrations up to 1 mM, but no NAD(P)H consumption was observed, in contrast to *Lc*DHFR, *Ec*DHFR, and *Hs*DHFR, which are capable of reducing folate (*17*, *28*). The product inhibition studies revealed a pattern identical to those previously reported for *Ec*DHFR, with THF and $NADP^+$ behaving as noncompetitive inhibitors when DHF is the varied substrate and as competitive inhibitors when NADH is varied (Table 1). In combination with the initial velocity results, this argues against a classic steady-state ordered mechanism with either pyridine nucleotide or DHF binding first. The analysis of the dependence of $^DV/K_{app}$ on the concentration of the cosubstrate, which provides insight into the mechanism, is discussed below.

pH−Rate Profiles. To improve our understanding of the role of acid−base catalysis during substrate binding and catalysis, we determined pH−rate profiles in the pH range of 5.0−8.5. Two kinetic parameters were evaluated, k_{cat}, which reports on all steps after the formation of the ternary complex capable of undergoing catalysis until the release of all products, and k_{cat}/K_m, which gives information about the binding of the varied substrate

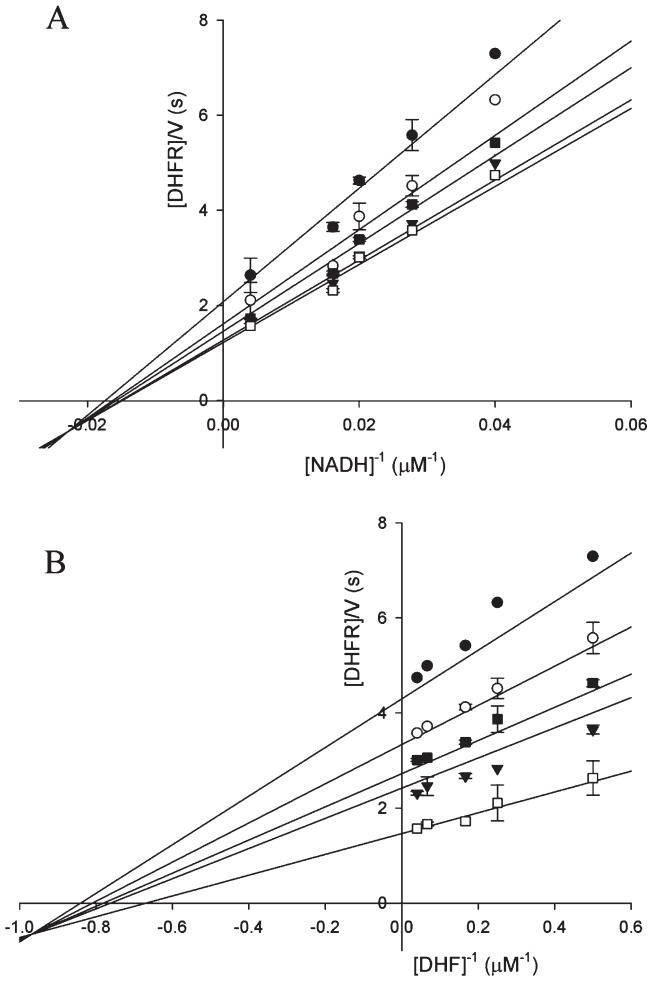

FIGURE 1: Initial velocity pattern showing lines intersecting to the left of the *y* axis. (A) NADH as the variable substrate and fixed DHF concentrations of 2 (●), 4 (○), 6 (▲), 15 (◆), and 25 μM (■). (B) DHF as the variable substrate and fixed NADH concentrations of 25 (●), 36 (○), 50 (▲), 62 (◆), and 250 μM (■). Global fitting of the data to eq 2 (—) gave the following: $k_{cat} = 1.65 \pm 0.10\ s^{-1}$, $K_{DHF} = 1.62 \pm 0.40\ \mu M$, and $K_{NADH} = 68.67 \pm 7.70\ \mu M$.

Table 1: Product Inhibition Patterns for *Mt*DHFR

varied substrate	product inhibitor	inhibition type[a]	K_{is} (μM)[b]	K_{ii} (μM)[c]
NADH	$NADP^+$	C	0.020 ± 0.005	–
NADH	THF	C	31 ± 3	–
DHF	$NADP^+$	NC	0.40 ± 0.10	0.10 ± 0.04
DHF	THF	NC	38 ± 5	13 ± 6

[a]C, competitive; NC, noncompetitive. [b]K_{is} is the slope inhibition constant. [c]K_{ii} is the intercept inhibition constant.

to the free enzyme. The pH dependence of k_{cat}, k_{cat}/K_{DHF}, and k_{cat}/K_{NADH} allowed the determination of pK_a values of 6.8 ± 0.2, 6.9 ± 0.1, and 7.0 ± 0.1, respectively (Figure 2), suggesting that a single group needs to be protonated for maximum substrate binding and/or catalysis. A comparison of the sequences of *Mt*DHFR with DHFRs from other organisms suggests that this residue is a conserved aspartate (Asp27) (*4*), and similar pH profiles have been reported for other DHFRs, yielding similar pK_a values (*29*). However, there is not a consensus in the literature about the exact role Asp27 plays in the catalytic mechanism of other DHFRs, and different alternatives have

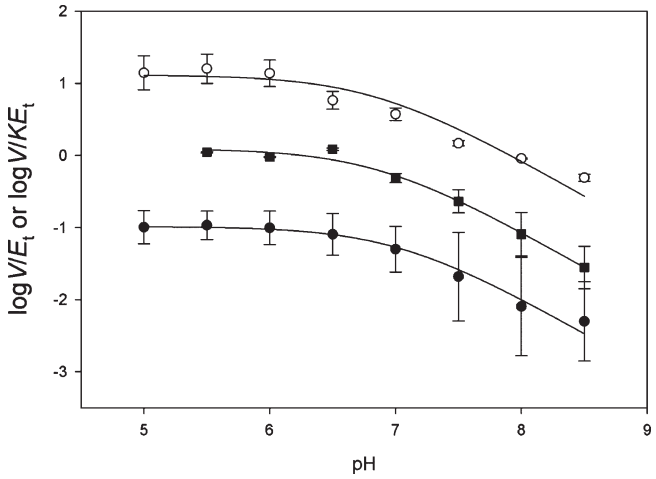

FIGURE 2: pH dependence of (A) log V/E_tK_{NADH} (○), (B) V/E_tK_{DHF} (■), and (C) V/E_t (●). The lines represent fits to eq 5. A mixed buffer system was utilized, with 100 mM citrate, 100 mM HEPES, and 100 mM TAPS.

been proposed (*30*, *31*). It is clear that Asp27 cannot be directly involved in protonation of N5 of the pteridine ring of DHF because they are separated by more than 5 Å [Protein Data Bank (PDB) entry 2CIG (*13*)]. It has also been suggested that when DHF is bound in the *Ec*DHFR active site, the N5 pK_a increases from < 3 when free in solution to a value of 6.0, indicating that the pK_a observed for this enzyme could be reflecting the pteridine N5 pK_a value, rather than Asp27 (*32*) We do not believe this is the case for the MtDHFR, because the protonation step would have to possess a somewhat rate-limiting nature to be observed in the pH−rate profiles, which was not observed in the solvent and multiple KIE studies (see below).

Primary Kinetic Isotope Effects. To investigate the rate-limiting nature of the chemical step, the pH dependence of primary kinetic isotope effects was measured. It is important to note that the values obtained here are observed KIEs, and it is unlikely that these values represent intrinsic KIEs. In the case of *Mt*DHFR, intrinsic KIEs report uniquely on the hydride transfer step, and these values are often masked by commitment factors in the forward and reverse directions. The forward commitment (c_f) represents the tendency of the enzyme complex capable of undergoing catalysis to continue forward as opposed to its tendency to dissociate to free enzyme and free substrate, and the reverse commitment (c_r) represents the same tendency for the reverse reaction (*33*). Examples of events in the catalytic cycle that raise commitment factors, consequently decreasing the magnitude of the observed KIE, are conformational changes, binding of substrates, release of products, and others (*33*). When [4*R*-4-^{2}H]NADH was used as the substrate, the KIEs increased: at pH 5.5, $^DV = 1.6 \pm 0.1$ and $^DV/K_{NADH} = 1.6 \pm 0.2$, and at pH 7.5, $^DV = 2.9 \pm 0.4$ and $^DV/K_{NADH} = 3.1 \pm 0.3$; $^DV/K_{DHF}$ remained 2.7 ± 0.3 throughout the pH range analyzed (Table 2 and Figure 3A). The observation that ^DV, $^DV/K_{NADH}$, and $^DV/K_{DHF}$ are statistically higher than unity suggests that the hydride transfer step is at least partly rate limiting throughout the pH range analyzed (*34*). The classical upper limit for deuterium primary KIEs, in cases where there is no tunneling, is ca. 7, and values of > 2 can be considered partially rate limiting for hydride transfer (*35*). When [4*R*-4-^{2}H]NADPH was used as the substrate (Table 3 and Figure 3B), the KIEs increased: at pH 5.5, $^DV = 1.0 \pm 0.1$ and $^DV/K_{DHF} = 1.6 \pm 0.2$, and at pH 8.0, $^DV = 2.3 \pm 0.1$ and $^DV/K_{DHF} = 2.9 \pm 0.2$. Because of the low value of

Table 2: Kinetic Isotope Effects Obtained with NADH as the Substrate

	pH (pD)	isotope effect
$^{D}V/K_{DHF}$	5.5	2.6 ± 0.3
$^{D}V/K_{NADH}$	5.5	1.6 ± 0.2
^{D}V	5.5	1.6 ± 0.1
$^{D}V/K_{DHF}$	6.0	2.2 ± 0.4
$^{D}V/K_{NADH}$	6.0	3.1 ± 0.3
^{D}V	6.0	2.0 ± 0.2
$^{D}V/K_{DHF}$	6.5	2.7 ± 0.1
$^{D}V/K_{NADH}$	6.5	2.5 ± 0.4
^{D}V	6.5	2.7 ± 0.1
$^{D}V/K_{DHF}$	7.5	2.6 ± 0.4
$^{D}V/K_{NADH}$	7.5	3.1 ± 0.3
^{D}V	7.5	3.2 ± 0.1
$^{D_2O}V/K_{DHF}$	6.0	0.9 ± 0.1
$^{D_2O}V/K_{NADH}$	6.0	0.8 ± 0.1
^{D_2O}V	6.0	0.8 ± 0.1
$^{D_2O}V/K_{[4R\text{-}4\text{-}^2H]NADH}$	6.0	0.6 ± 0.1
$^{D_2O}V_{[4R\text{-}4\text{-}^2H]NADH}$	6.0	0.7 ± 0.1
$^{D}K_{eq}$	6.0	1.14 ± 0.08
$^{D_2O}K_{eq}$	6.0	1.03 ± 0.01

K_{NADPH}, $^{D}V/K_{NADPH}$ could not be reliably measured. The lower observed KIE values obtained when NADPH was used as the substrate instead of NADH suggest that NADPH is a stickier substrate than NADH. A sticky substrate is a substrate that reacts to form products faster than it dissociates from the enzyme, increasing the c_f and consequently decreasing the observed KIEs (*36*). Additionally, the slightly lower value of ^{D}V relative to the $^{D}V/K_{DHF}$ when NADPH was the cosubstrate suggests that a step after the first irreversible step, often considered to be the release of the first product, is contributing to the rate (*34*). In the reactions catalyzed by *Ec*DHFR (*37*), *Hs*DHFR (*24*), and *Lactobacillus casei* [*Lc*DHFR (*38*)], the rate-limiting step is THF release and the chemical step is not rate-limiting at neutral pH (*37*). In the DHFR from *S. pneumoniae* (*Sp*DHFR), it was suggested that the k_{cat} at pH 7 was limited by a slow conformational change prior to the chemical step and the actual hydride transfer step (*25*), and that product release was not rate-limiting at any of the pH values analyzed.

Furthermore, pK_a values of 7.4 ± 0.1 and 6.3 ± 0.3 for ^{D}V and $^{D}V/K_{DHF}$, respectively, were observed when the pH dependence of the KIEs using NADPH as the substrate was analyzed (Figure 3B). These values are comparable to those obtained in the pH−rate profiles discussed above, suggesting that the same group that needs to be protonated for maximum binding and catalysis is also influencing the magnitude of the observed KIEs. When the pH is low, the chemical step is faster than another step that partially limits the rate, and the observed KIEs are close to unity. As the pH increases, the hydride transfer step slows and becomes rate-limiting, thus increasing the magnitude of the observed KIEs.

While NADPH is sticky compared to NADH, and presumably DHF, the relative stickiness of DHF and NADH was determined by the analysis of the dependence of the apparent isotope effect on V/K on the concentration of the cosubstrate. Theory predicts that the magnitude of $^{D}V/K_{app}$ will be dependent on the order of addition of substrates, and specific patterns of codependence are expected for a given mechanism (*39*). In this model, A represents the first substrate to bind in an ordered mechanism and B is the second substrate to bind. In steady-state ordered mechanisms, $^{D}(V/K_{app})_B$ will be independent of the concentration of A while $^{D}(V/K_{app})_A$, if A is sticky, will decrease as the concentration of B is increased and become unity at an infinite concentration of B. The pattern is similar in steady-state random mechanisms, but $^{D}V/K_{app}$ for a sticky substrate will decrease as the concentration of the cosubstrate is increased and reach a finite value different from that at an infinite concentration of the cosubstrate. For a nonsticky substrate, $^{D}V/K_{app}$ will be independent of the concentration of the cosubstrate. In the case of mechanisms of the rapid equilibrium

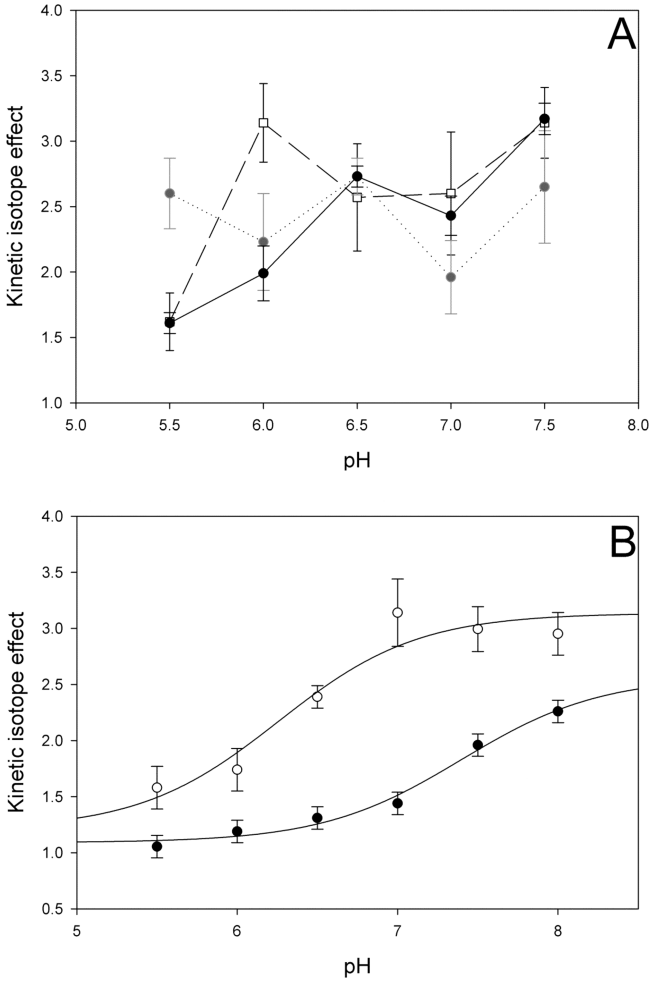

FIGURE 3: pH dependence of the kinetic isotope effects when (A) NADH or (B) NADPH was used as the substrate. The individual values represent fits to eq 7 and are the average of at least two independent experiments. A mixed buffer system was utilized, with 100 mM citrate, 100 mM HEPES, and 100 mM TAPS. (A) pH dependence of ^{D}V (●), $^{D}V/K_{NADH}$ (□), and $^{D}V/K_{DHF}$ (gray circles). (B) pH dependence of ^{D}V (●) and $^{D}V/K_{DHF}$ (○). The line is a fit to eq 6.

Table 3: Kinetic Isotope Effects Obtained with NADPH as the Substrate

	pH (pD)	isotope effect
$^{D}V/K_{DHF}$	5.5	1.6 ± 0.2
^{D}V	5.5	1.1 ± 0.1
$^{D}V/K_{DHF}$	6.0	1.7 ± 0.2
^{D}V	6.0	1.2 ± 0.1
$^{D}V/K_{DHF}$	6.5	2.4 ± 0.1
^{D}V	6.5	1.3 ± 0.1
$^{D}V/K_{DHF}$	7.0	3.1 ± 0.3
^{D}V	7.0	1.4 ± 0.1
$^{D}V/K_{DHF}$	7.5	3.0 ± 0.2
^{D}V	7.5	2.0 ± 0.1
$^{D}V/K_{DHF}$	8.0	3.0 ± 0.2
^{D}V	8.0	2.3 ± 0.1
$^{D}k_H$	5.5	2.4 ± 0.1
$^{D}k_H$	7.5	2.7 ± 0.1

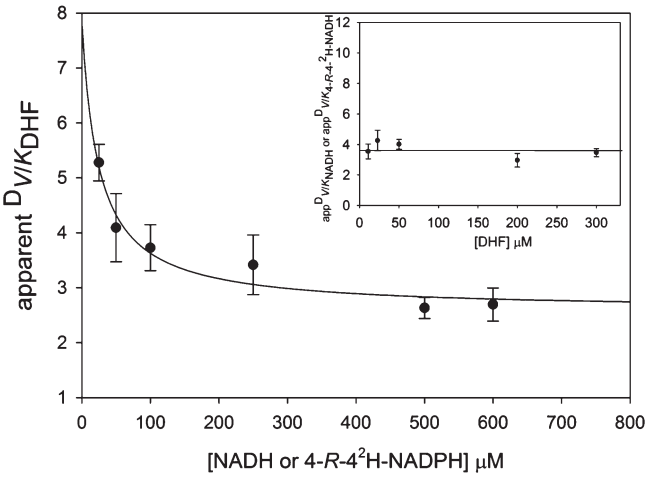

FIGURE 4: Dependence of the apparent values of $^{D}V/K$ on the concentration of the cosubstrate. KIEs were measured by varying the concentration of DHF at five different fixed concentrations of NADH or [4*R*-4-^{2}H]NADH. Assays contained 100 mM HEPES (pH 7.5) with 50 mM KCl, DHFR (10−20 nM), DHF, and either NADH or [4*R*-4-^{2}H]NADH. The solid line drawn through $_{app}V/K_{DHF}$ is a fit to the relationship $^{D}V/K_{app} = {}^{D}V/K_{[NADL]\to\infty} + K(^{D}V/K_{NADL\to 0} - {}^{D}V/K_{NADL\to\infty})/(K + [NADL])$, where K is the concentration of NADL that gives $^{D}V/K_{app} = (^{D}V/K_{NADL\to 0} - {}^{D}V/K_{NADL\to\infty})/2$.

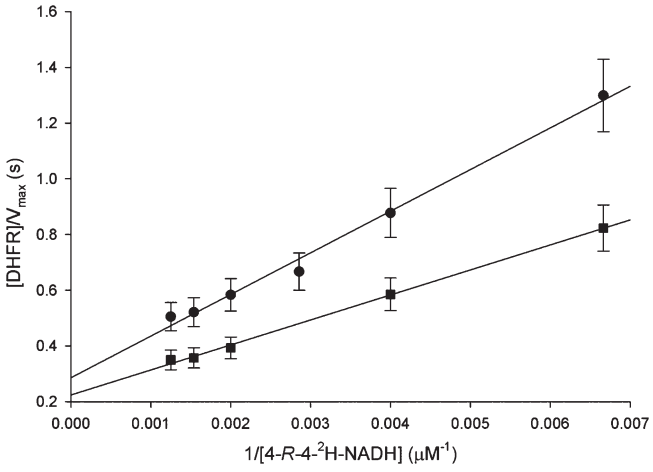

FIGURE 5: Multiple KIEs. Curves using [4*R*-4-^{2}H]NADH as the substrate and either H_2O (●) or D_2O (■) were compared. The concentration of [4*R*-4-^{2}H]NADH was varied while the concentration of DHF kept constant at 50 μM. Assays contained 100 mM citrate (pH 6.0) with 50 mM KCl, DHFR (10−20 nM), DHF, and [4*R*-4-^{2}H]NADH.

type, both ordered or random, $^{D}V/K_{app}$ for the two substrates will be equal and independent of the concentration of the cosubstrate because all external commitment factors are zero (*38*).

In our case, $^{D}(V/K_{app})_{NADH}$ was independent of the concentration of DHF and exhibited a value of > 1, while $^{D}(V/K_{app})_{DHF}$ decreased hyperbolically as the concentration of NADL increased, reaching a constant value of > 1 at elevated concentrations of NADL (Figure 4). This pattern is characteristic of a steady-state random mechanism, as observed in other reductases, including 1-deoxy-D-xylulose-5-phosphate isomeroreductase and β-ketoacyl-acyl carrier protein (ACP) reductase, both from *M. tuberculosis* (*40*, *41*). This result also indicates that DHF is a sticky substrate when the reaction occurs with NADH, and that NADH is less sticky than DHF. It is important to point out that the *Mt*DHFR is copurified with NADPH tightly bound, indicating that even though the free enzyme is physically capable of binding both substrates randomly, it is likely that there is a preferential pathway favoring NADPH binding first.

Solvent and Multiple Kinetic Isotope Effects. To investigate the rate-limiting nature of the protonation step, solvent KIEs were measured at pH 6.0, and all values were slightly inverse [$^{D_2O}V/K_{DHF} = 0.9 \pm 0.1$, $^{D_2O}V/K_{NADH} = 0.8 \pm 0.1$, and $^{D_2O}V = 0.8 \pm 0.1$ (Table 2)]. A viscosity study using 9% glycerol to mimic the relative viscosity of D_2O was conducted, and no effect of viscosity on the rate was observed (data not shown). This result shows that the protonation step is not rate-limiting at this pH, when NADH and DHF are the substrates. To discriminate between a concerted and stepwise mechanism for proton and hydride transfer, multiple kinetic isotope effects were determined, measuring the solvent KIE when [4*R*-4-^{2}H]NADH and DHF were used as substrates (Figure 5). In this experiment, statistically significant inverse values of $^{D_2O}V/K_{[4R\text{-}4\text{-}^{2}H]NADH}$ (0.6 ± 0.1) and ^{D_2O}V (0.7 ± 0.1) were found. According to theory (*42*), if protonation and hydride transfer were occurring in the same transition state, i.e., in a concerted manner, the observed multiple KIE would be equal or greater in magnitude than the solvent KIE, because the presence of deuterium in the multiple KIE experiment would increase the relative size of the energy barrier for the hydride transfer, consequently increasing the energy barrier for protonation. On the other hand, if protonation and hydride transfer were taking place in a stepwise manner, the observed multiple KIE would be smaller than the solvent KIE, because the energy barrier for hydride transfer would be higher, decreasing the observed KIE when water and D_2O are compared. Hence, the results presented here suggest that the reaction follows a stepwise mechanism, and that protonation and hydride transfer are not part of the same transition state. The fact that the multiple KIE yielded an inverse value suggests that a fast pre-equilibrium protonation is occurring before the hydride transfer step (*35*). Because heavy water influences acid−base equilibria, D_2O being more acidic than H_2O, one can imagine that the presence of a fast pre-equilibrium protonation preceding the relatively slower hydride transfer step could give rise to the observed inverse multiple KIEs due to the fact that the rapid protonation would increase the amount of an N5-protonated intermediate, which would be the true "substrate" for the hydride transfer (Scheme 2). Furthermore, inverse fractionation factors have been measured for several few amines, revealing that some solvent-exchangeable sites prefer deuterium over hydrogen, relative to solvent, which could also contribute to the inverse values obtained here (*43*, *44*).

Equilibrium Isotope Effects (*EIE*). Even though the results presented above indicate that a fast pre-equilibrium protonation is occurring prior to the hydride transfer step, EIE ($^{D}K_{eq}$ and $^{D_2O}K_{eq}$) were measured to better corroborate this mechanism. If there are isotope effects reporting on the hydride transfer step [$^{D}(V/K)_{NADH}$], the protonation step [$^{D_2O}(V/K)_{NADH}$], and both [$^{D_2O}(V/K)_{[4R\text{-}4\text{-}^{2}H]NADPH}$], those values can be used in combination with $^{D}K_{eq}$ and $^{D_2O}K_{eq}$ to provide information about which one of these steps comes first. The following values were obtained at pH 6.0: $^{D}K_{eq} = 1.14 \pm 0.08$, and $^{D_2O}K_{eq} = 1.03 \pm 0.01$. To distinguish between protonation preceding or following hydride transfer, we must satisfy the following inequality:

$$^{D}K_{eq} \neq \frac{[^{D_2O}(V/K)_{NADH} - {}^{D_2O}K_{eq}][^{D_2O}(V/K)_{[4R-4-^{2}H]NADH} - 1]}{[^{D_2O}(V/K)_{NADH} - 1][^{D_2O}(V/K)_{[4R-4-^{2}H]NADH} - {}^{D_2O}K_{eq}]}$$

If the two sides of this equation were equal, the two mechanisms could not be distinguished by the analysis of multiple and

Scheme 2: Chemical Mechanism Proposed for the *Mt*DHFR-Catalyzed Reaction[a]

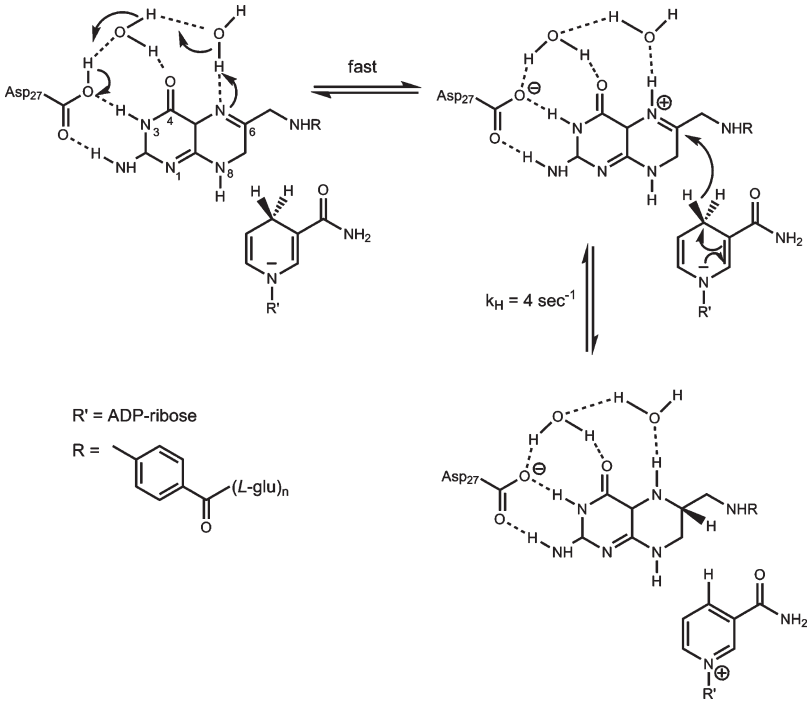

[a]Asp27 is protonated as indicated by the pH−rate profiles. A conserved water molecule is shown participating in hydrogen bonds with O4 and Asp27. N5 protonation is fast and mediated by a solvent molecule. The preprotonated intermediate is then attacked by NAD(P)H, forming the products THF and NAD(P)$^+$.

equilibrium KIEs (*42*). Unfortunately, this is the case for the *Mt*DHFR-catalyzed reaction.

Several theoretical studies indicate that the mechanism in which protonation precedes hydride transfer is energetically favored, at least for the *Ec*DHFR (*7*, *8*). In this model, DHF binds the enzyme in its unprotonated form, and the enzyme facilitates protonation by exposing N5 to the solvent in a favorable orientation, in a hydrophobic pocket that locally increases the N5 pK_a (*9*). Additionally, it was previously demonstrated by deuterium exchange experiments that the proton on N5, in the *Ec*DHFR, comes from the solvent (*7*), corroborating the mechanism proposed here for the *Mt*DHFR-catalyzed reaction (Scheme 2).

Primary KIEs under Pre-Steady-State Conditions. The reaction rate was measured under single-turnover conditions to obtain more detailed information about the hydride transfer step. When single-turnover experiments are performed, the rate obtained is a combination of the rates of binding and dissociation, and forward and reverse chemical reactions. By varying the concentration of enzyme, one expects that the rate of binding becomes fast at the maximal enzyme concentration, allowing the observed rates obtained with different concentrations of enzyme to be plotted as a function of enzyme concentration, yielding a hyperbola whose y_{max} can the interpreted as the rate of the chemical step. In the case of *Mt*DHFR, k_H will be used to describe the hydride transfer step when NADPH is used as the substrate and k_D when [4*R*-4-^{2}H]NADPH is the substrate. The values obtained for k_H were 8.8 ± 0.1 and 4.0 ± 0.7 s^{-1} at pH 5.5 and 7.5, respectively. Interestingly, the k_H values measured here are only slightly higher than k_{cat}, illustrating the overall rate-limiting nature of the hydride transfer step in the pH range analyzed. These values are 2 orders of magnitude smaller than those for *Ec*DHFR, *Hs*DHFR, and *Lc*DHFR, at both pH 5.5 and 7.5. To rule out the possibility that a conformational change occurring prior to k_H is limiting the reaction, kinetic isotope effects were measured under single-turnover conditions. If a rate-limiting slower step was occurring prior to k_H, the values of kinetic isotope effects on the hydride transfer step (^Dk_H) would have a decreased magnitude, because of the presence of a high c_f. The value obtained for ^Dk_H at pH 5.5 was 2.4 ± 0.1, very similar to the value obtained at pH 7.5 [^Dk_H = 2.7 ± 0.3 (Figure 6)]. Thus, the possibility that a conformational change prior to the chemical step is determining k_{cat} was ruled out, because the

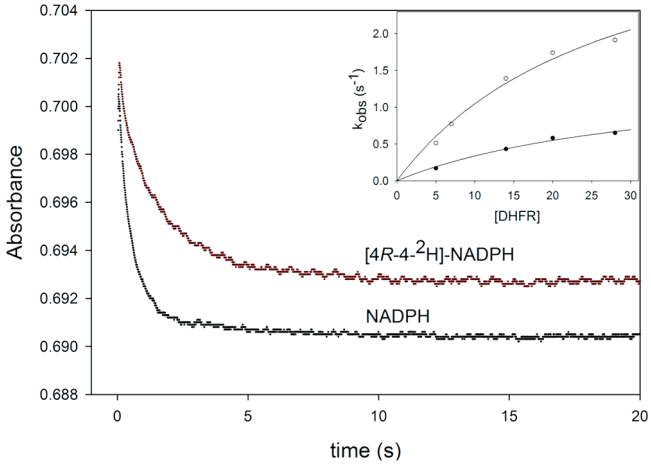

FIGURE 6: KIEs under single-turnover conditions. Each curve represents the average of seven traces collected with 20 μM DHFR, 1 μM DHF, and 100 μM NADPH or 100 μM [4*R*-4-^{2}H]NADPH, at pH 7.5. The straight line represents a fit to a single-exponential decay (eq 9). The inset shows the replot of the observed rate constants (k_{obs}) obtained with 5, 7, 14, 20, and 28 μM DHFR, and either NADPH (○) or [4*R*-4-^{2}H]NADPH (●). The lines represent the fits to eq 10.

magnitude of $^{D}k_{H}$ would be decreased if that were the case. These results are in contrast to what was found in the DHFR from *S. pneumoniae* (*Sp*DHFR), where the k_H/k_D was unity at pH 6.0 and 2.4 at pH 7.0 (*25*), and in agreement with the values obtained for the *Ec*DHFR-catalyzed reaction (*37*).

Furthermore, the values obtained for $^{D}k_{H}$ are very comparable to all $^{D}V/K$ values obtained at pH 7.5, when both NADH and NADPH were used as substrates. In this situation, one can be tempted to interpret the value of ≈2.7 as the intrinsic KIE ($^{D}k_{chem}$) for this enzyme-catalyzed reaction, because $^{D}V/K$ and $^{D}k_{H}$ can be considered equal within experimental error, as illustrated by the equation defining $^{D}V/K$ isotope effects shown below:

$$^{D}V/K = \frac{^{D}k + c_f + c_r \times {}^{D}K_{eq}}{1 + c_f + c_r}$$

This assumption, even though plausible, must be taken with caution, because it is possible that both $^{D}V/K$ and $^{D}k_{H}$ are being decreased from the true intrinsic value by the same factor. The intrinsic KIE was experimentally determined for *Ec*DHFR, being equal to 3.5 ± 0.2, and the c_f was then calculated to be 0.25 (*45*).

In this work, the kinetic mechanism of the *Mt*DHFR-catalyzed reaction was determined to be steady-state random, with a preferred pathway in which NADPH binds first. A pK_a value of approximately 7.0 was identified for an enzymic acid, and kinetic isotope effects revealed the partly rate limiting nature of the hydride transfer step from pH 5.5 to 8.0. Kinetic isotope effects were measured for the hydride transfer step, and EIE were measured for the first time for this reaction. A chemical mechanism including a pre-equilibrium protonation step preceding the hydride transfer step was suggested. Future studies include a complete pre-steady-state analysis to improve our understanding of the catalytic cycle of the *Mt*DHFR-catalyzed reaction, as well as a study of mutants aimed at improving our understanding of the role of specific amino acids in catalysis.

ACKNOWLEDGMENT

We thank Paul F. Cook (University of Oklahoma, Norman, OK) for his valuable advice and assistance in the interpretation of the kinetic isotope effects and Argyrides Argyrou (GlaxoSmithKline) for his help with data analysis.

SUPPORTING INFORMATION AVAILABLE

A multiple-sequence alignment of DHFRs from several sources, a structure-based sequence alignment of the *E. coli* and *M. tuberculosis* DHFRs, and a structural overlay of the three-dimensional structures of the *E. coli* and *M. tuberculosis* DHFRs. This material is available free of charge via the Internet at http://pubs.acs.org.

REFERENCES

1. Global tuberculosis control: Epidemiology, strategy, financing: WHO Report 2009. http://www.who.int/tb/publications/global_report/2009/en/index.html (accessed August 15, 2010).
2. Dye, C., Williams, B. G., Espinal, M. A., and Raviglione, M. C. (2002) Erasing the world's slow stain: Strategies to beat multidrug-resistant tuberculosis. *Science 295*, 2042–2046.
3. Kompis, I. M., Islam, K., and Then, R. L. (2005) DNA and RNA Synthesis: Antifolates. *Chem. Rev. 105*, 593–620.
4. Li, R., Sirawaraporn, R., Chitnumsub, P., Sirawaraporn, W., Wooden, J., Athappilly, F., Turley, S., and Hol, W. G. J. (2000) Three-dimensional Structure of *M. tuberculosis* Dihydrofolate Reductase Reveals Opportunities for the Design of Novel Tuberculosis Drugs. *J. Mol. Biol. 295*, 307–323.
5. El-Hamamsy, M. H. R. I., Smith, A. W., Thompson, A. S., and Threadgill, M. D. (2007) Structure-based design, synthesis and preliminary evaluation of selective inhibitors of dihydrofolate reductase from *Mycobacterium tuberculosis*. *Bioorg. Med. Chem. 15*, 4552–4576.
6. Kumar, A., and Siddiqi, M. I. (2008) Virtual screening against *Mycobacterium tuberculosis* dihydrofolate reductase: Suggested workflow for compound prioritization using structure interaction fingerprints. *J. Mol. Graphics Modell. 27*, 476–488.
7. Deng, H., and Callender, R. (1998) Structure of Dihydrofolate When Bound to Dihydrofolate Reductase. *J. Am. Chem. Soc. 120*, 7730–7737.
8. Gready, J. E. (1985) Theoretical Studies on the Activation of the Pterin Cofactor in the Catalytic Mechanism of Dihydrofolate Reductase. *Biochemistry 24*, 4761–4766.
9. Rod, T. H., and Brooks, C. L. (2003) How Dihydrofolate Reductase Facilitates Protonation of Dihydrofolate. *J. Am. Chem. Soc. 125*, 8718–8719.
10. Shrimpton, P., and Allemann, R. K. (2002) Role of water in the catalytic cycle of *E. coli* dihydrofolate reductase. *Protein Sci. 11*, 1442–1451.
11. Morrison, J. F., and Stone, S. R. (1988) Mechanism of the reaction catalyzed by dihydrofolate reductase from *Escherichia coli*: pH and deuterium isotope effects with NADPH as the variable substrate. *Biochemistry 27*, 5499–5506.
12. Loveridge, E. J., Behiry, E. M., Swanwick, R. S., and Allemann, R. K. (2009) Different Reaction Mechanisms for Mesophilic and Thermophilic Dihydrofolate Reductases. *J. Am. Chem. Soc. 131*, 6926–6927.
13. Argyrou, A., Vetting, M. W., Aladegbami, B., and Blanchard, J. S. (2006) *Mycobacterium tuberculosis* dihydrofolate reductase is a target for isoniazid. *Nat. Struct. Mol. Biol. 13*, 408–413.
14. Pace, C. N., Vajdos, F., Fee, L., Grimsley, G., and Gray, T. (1995) How to measure and predict the molar absorption coefficient of a protein. *Protein Sci. 4*, 2411–2423.
15. Ottolina, G., Riva, S., Carrea, G., Danieli, B., and Buckmann, A. F. (1989) Enzymatic synthesis of [4*R*-4-^{2}H]NAD(P)H and [4*S*-4-^{2}H]-NAD(P)H and determination of the stereospecificity of 7α- and 12α-hydroxysteroid dehydrogenase. *Biochim. Biophys. Acta 998*, 173–178.
16. Jeong, S., and Gready, J. E. (1994) A method of preparation and purification of (4*R*)-deuterated-reduced nicotinamide adenine dinucleotide phosphate. *Anal. Biochem. 221*, 273–277.
17. Stone, S. R., and Morrison, J. F. (1982) Kinetic mechanism of the reaction catalyzed by dihydrofolate reductase from *Escherichia coli*. *Biochemistry 21*, 3757–3765.
18. Karsten, W. E., Lai, C., and Cook, P. F. (1995) Inverse Solvent Isotope Effects in the NAD-Malic Enzyme Reaction Are the Result of the Viscosity Difference between D_2O and H_2O: Implications for Solvent Isotope Effect Studies. *J. Am. Chem. Soc. 117*, 5914–5918.
19. Cook, P. F., Blanchard, J. S., and Cleland, W. W. (1980) Primary and Secondary Deuterium Isotope Effects on Equilibrium Constants for Enzyme-Catalyzed Reactions. *Biochemistry 21*, 4853–4858.
20. Reed, L. S., and Archer, M. C. (1980) Oxidation of Tetrahydrofolic Acid by Air. *J. Agric. Food Chem. 28*, 801–805.
21. Francis, K., and Gadda, G. (2006) Probing the Chemical Steps of Nitroalkane Oxidation Catalyzed by 2-Nitropropane Dioxygenase with Solvent Viscosity, pH, and Substrate Kinetic Isotope Effects. *Biochemistry 45*, 13889–13898.
22. Northrop, D. B. (1975) Steady-state analysis of kinetic isotope effects in enzymic reactions. *Biochemistry 14*, 2644–2651.
23. Hiromi, K. (1979) Kinetics of Fast Enzyme Reactions, pp 346, John Wiley and Sons, Inc., New York.
24. Appleman, J. R., Beard, W. A., Delcampg, T. J., Prendergast, N. J., Freisheimg, J. H., and Blakley, R. L. (1990) Unusual Transient- and Steady-state Kinetic Behavior Is Predicted by the Kinetic Scheme Operational for Recombinant Human Dihydrofolate Reductase. *J. Biol. Chem. 265*, 2740–2748.
25. Lee, J., Yennawar, N. H., Gam, J., and Benkovic, S. J. (2010) Kinetic and Structural Characterization of Dihydrofolate Reductase from *Streptococcus pneumonia*. *Biochemistry 49*, 195–206.
26. Thillet, J., Adams, J. A., and Benkovic, S. J. (1990) The kinetic mechanism of wild-type and mutant mouse dihydrofolate reductases. *Biochemistry 29*, 5195–5202.
27. Huang, S., Appleman, J. R., Tan, X., Thompson, P. D., Blakley, R. L., Sheridan, R. P., Venkataraghavan, R., and Freisheim, J. H. (1990) Role of Lysine-54 in Determining Cofactor Specificity and Binding in Human Dihydrofolate Reductase. *Biochemistry 29*, 8063–8069.

28. Williams, E. A., and Morrison, J. F. (1992) Human dihydrofolate reductase: Reduction of alternative substrates, pH effects, and inhibition by deazafolates. *Biochemistry 31*, 6801–6811.
29. Beard, W. A., Appleman, J. R., Delcamp, T. J., Freisheims, J. H., and Blakley, R. L. (1989) Hydride Transfer by Dihydrofolate Reductase. *J. Biol. Chem. 264*, 9391–9399.
30. Deng, H., and Callender, R. (1998) Structure of Dihydrofolate When Bound to Dihydrofolate Reductase. *J. Am. Chem. Soc. 120*, 7730–7737.
31. Gready, J. E. (1985) Theoretical Studies on the Activation of the Pterin Cofactor in the Catalytic Mechanism of Dihydrofolate Reductase. *Biochemistry 24*, 4761–4766.
32. Chen, Y. Q., Kraut, J., Blakley, R. L., and Callender, R. (1994) Determination by Raman Spectroscopy of the p*Ka* of N5 of Dihydrofolate Bound to Dihydrofolate Reductase: Mechanistic Implications. *Biochemistry 33*, 7021–7026.
33. Northrop, D. B. (1981) The expression of isotope effects on enzyme-catalyzed reactions. *Annu. Rev. Biochem. 50*, 103–131.
34. Cook, P. F. (1991) in Enzyme Mechanism from Isotope Effects, pp 432, CRC Press, Boca Raton, FL.
35. Wiberg, K. B. (1955) The Deuterium Isotope Effect. *Chem. Rev. 55*, 713–743.
36. Cook, P. F., and Cleland, W.W. (2007) in Enzyme kinetics and mechanism, pp 416, Garland Science, New York.
37. Fierke, C. A., Johnson, K. A., and Benkovic, S. J. (1987) Construction and Evaluation of the Kinetic Scheme Associated with Dihydrofolate Reductase from *Escherichia coli*. *Biochemistry 26*, 4085–4092.
38. Andrews, J., Fierke, C. A., Birdsall, B., Ostler, G., Feeney, J., Roberts, G. C., and Benkovic, S. J. (1989) A kinetic study of wild-type and mutant dihydrofolate reductases from *Lactobacillus casei*. *Biochemistry 28*, 5743–5750.
39. Cook, P. F., and Cleland, W. W. (1981) Mechanistic Deductions from Isotope Effects in Multireactant Enzyme Mechanisms. *Biochemistry 20*, 1790–1796.
40. Argyrou, A., and Blanchard, J. S. (2004) Kinetic and Chemical Mechanism of *Mycobacterium tuberculosis* 1-Deoxy-D-xylulose-5-phosphate isomeroreductase. *Biochemistry 43*, 4375–4384.
41. Silva, R. G., de Carvalho, L. P. S., Blanchard, J. S., Santos, D. S., and Basso, L. A. (2006) *Mycobacterium tuberculosis* β-ketoacyl-acyl carrier protein (ACP) reductase: Kinetic and chemical mechanisms. *Biochemistry 45*, 13064–13073.
42. Hermes, J. D., Roeske, C. A., O'Leary, M. H., and Cleland, W. W. (1982) Use of multiple isotope effects to determine enzyme mechanisms and intrinsic isotope effects. Malic enzyme and glucose-6-phosphate dehydrogenase. *Biochemistry 21*, 5106–5114.
43. Reuben, J. (1986) Deuterium/Protium fractionation factors for polyfunctional organic molecules: Direct determination by carbon-13 NMR spectroscopy. *J. Am. Chem. Soc. 108*, 1082–1083.
44. Vakonakis, I., Salazar, M., Kang, M., Dunbar, K. R., and LiWang, A. C. (2003) Deuterium isotope effects and fractionation factors of hydrogen-bonded A:T base pairs of DNA. *J. Biomol. NMR 25*, 105–112.
45. Sikorski, R. S., Wang, L., Markham, K. A., Pajagopalan, P. T., Benkovic, S. J., and Kohen, A. (2004) Tunneling and coupled motions in the *Escherichia coli* dihydrofolate reductase catalysis. *J. Am. Chem. Soc. 126*, 4778–4779.